Massive Star Formation: Observations Confront Theory
ASP Conference Series, Vol. 387, ©2008
H. Beuther, H. Linz, and Th. Henning, eds.

Dissecting Massive YSOs with Mid-Infrared Interferometry

H. Linz[1], Th. Henning[1], B. Stecklum[2], A. Men'shchikov[3], R. van Boekel[1], R. Follert[2], M. Feldt[1]

Abstract. The very inner structure of massive YSOs is difficult to trace. With conventional observational methods we often identify structures still several hundreds of AU in size. But we also need information about the innermost regions where the actual mass transfer onto the forming high-mass star occurs. An innovative way to probe these scales is to utilise mid-infrared interferometry. Here, we present first results of our MIDI GTO programme at the VLTI. We observed 10 well-known massive YSOs down to scales of 20 mas. We clearly resolve these objects which results in low visibilities and sizes in the order of 30 – 50 mas. Thus, with MIDI we can for the first time quantify the extent of the thermal emission from the warm circumstellar dust and thus calibrate existing concepts regarding the compactness of such emission in the pre-UCHII region phase. Special emphasis will be given to the BN-type object M8E-IR where our modelling is most advanced and where there is indirect evidence for a strongly bloated central star.

1. Introduction

High-mass stars predominantly form in clustered environments much farther away from the Sun, on average, than typical well-investigated low-mass star-forming regions. Thus, high spatial resolution is a prerequisite for making progress in the observational study of high-mass star formation. Furthermore, all phases prior to the main sequence are usually deeply embedded. This often forces observers of deeply embedded massive young stellar objects (MYSOs) to move to the mid-infrared (MIR) where the resolution of conventional imaging is limited to $> 0\farcs25$ even with 8-m class telescopes. Hence, one traces linear scales still several hundred AU in size even for the nearest MYSOs, and conclusions on the geometry of the innermost circumstellar material remain ambiguous. MIR emission moderately resolved with single-dish telescopes could even arise from the inner outflow cones (e.g., De Buizer 2006; Linz et al. 2005).
The most versatile method to overcome the diffraction limit of single telescopes is to employ interferometric techniques. We are presently conducting a larger survey toward MYSOs based on MIR interferometry. In total, we have observed 10 sources so far. All these sources, mostly comprising BN-type objects (cf.

[1]Max–Planck–Institut für Astronomie Heidelberg, Königstuhl 17, 69117 Heidelberg, Germany

[2]Thüringer Landessternwarte Tautenburg, Sternwarte 5, 07778 Tautenburg, Germany

[3]CEA Saclay/DSM/DAPNIA, Service d'Astrophysique, Orme des Merisiers, Bat. 709, F-91191 Gif-sur-Yvette Cedex, France

Henning 1990), are clearly resolved with the interferometer baselines we applied (> 40 m). This in itself is a major step forward compared to the previous more or less unresolved thermal infrared imaging with 4-m to 8-m class telescopes for these sources. For this contribution, we concentrate on the object M8E-IR. This is a prominent BN-type MYSO at a distance of roughly 1.5 kpc[1] according to Simon et al. (1984). Although M8E-IR was a well investigated object in the 1980's, the spatial resolution for most of the IR observations of M8E-IR was limited. An exception is the work by Simon et al. (1985) who speculated on the existence of a small circumstellar disk around M8E-IR based on thermal infrared lunar occultation data.

2. MIDI interferometry for M8E–IR

Interferometric data in the mid-infrared wavelength range 8–13 μm have been obtained with the two-element interferometer MIDI (Leinert et al. 2003) at the Very Large Telescope Interferometer (VLTI). Within the framework of Guaranteed Time Observations (GTO) and Director's Discretionary Time (DDT) for MIDI, we observed M8E-IR at seven baseline length / baseline orientation combinations between June 2004 and June 2005. In Table 1 we summarise the observations. We list the UT dates and times for the fringe track data, the projected baseline lengths and the position angles of the projected baselines on the sky (counted from north over east on the sky), as well as the used telescope configurations and the observing proposal numbers. We refer to Leinert et al. (2004) for a more detailed description of the standard observing procedure for MIDI observations. For all our observations, the so-called HighSens mode was used: during self-fringe tracking, all the incoming thermal infrared signal is used for beam combination and fringe tracking, while the spectro-photometry is subsequently obtained in separate observations. We used the MIDI prism as the dispersing element to get spectrally dispersed visibilities ($R \approx 30$). HD 169916 was used as the main interferometric and photometric standard star and was observed always immediately after M8E-IR. In addition, all calibrator measurements of a night were collected to create an average interferometric transfer function and to assign error margins to the measured visibilities. For the August 01, 2004 observations, the conditions were almost photometric, and the airmass during the observations of both, M8R-IR and HD 169916 was minimal (1.01). Therefore, we used the dispersed photometry from this measurement to provide the N-band spectrum later used in the SED fitting (see Sect. 3.2.).

3. Results for M8E–IR

To have a fresh look on M8E–IR in its environment, we obtained Subaru/COMICS (Okamoto et al. 2003) thermal infrared imaging of this source from the SMOKA data archive (Baba et al. 2002). We show the corresponding 24.5 μm Subaru/COMICS image in Fig. 1 (Left). M8E-IR is still the dominating source

[1]Note, however, Arias et al. (2007) for suggesting $d = 1.25$ kpc for the M8 star clusters.

at this wavelength. At a nominal resolution of 0.″75, the emission remains compact. A second faint point source not yet reported in the literature is visible roughly 6″ west of it. Furthermore, we clearly detect MIR emission arising from the neighbouring radio source (Simon et al. 1984; Molinari et al. 1998). Simon et al. (1985) had already reported a detection of this source in N- and Q-band (fluxes only, measured with a 6″ diaphragm). For the first time, the Subaru MIR imaging spatially resolves this emission. It is cometary-shaped, with the apex directed away from M8E-IR. This morphology could be an intrinsic property of this UCHII region, or it could be shaped by the molecular outflow probably (arising from M8E-IR, Mitchell et al. (1988, 1992)) influencing this radio source. At 10.5 μm we easily detect M8E-IR, but the radio source counterpart is not detected (rms noise $\approx$ 4 mJy). Considering the COMICS filter characteristics, combined with the fact that the radio counterpart was detected by Simon et al. (1985) with 0.97 Jy in a broad N-band filter, this implies a very strong and broad 9.7 μm Silicate absorption feature. The third source in the 24.5 μm image is detected at a 4σ level at 10.5 μm.

Table 1. Log of MIDI observations of M8E-IR.

UT date and time	B [m]	PA [deg]	Telescope pair	ESO Program
2004-06-05 08:06:57	96.8	+42.7	U1–U3	073.C-0175(A)
2004-06-05 09:57:23	82.2	+44.5	U1–U3	073.C-0175(A)
2004-08-01 01:50:41	46.6	+38.4	U2–U3	273.C-5044(A)
2005-03-02 08:58:04	46.8	−85.9	U3–U4	074.C-0389(B)
2005-06-24 07:36:50	51.6	−42.2	U3–U4	075.C-0755(B)
2005-06-24 09:28:58	43.4	−10.6	U3–U4	075.C-0755(B)
2005-06-26 00:26:11	55.7	−06.6	U1–U2	075.C-0755(A)

3.1. MIR interferometry

We have reduced the interferometric data with the MIA+EWS package, version 1.5, developed at the MPIA Heidelberg and the University of Leiden. The resulting visibility curves are collected in Fig. 2 (Left). Starting from these curves we can already make some statements. The object is clearly resolved in all our configurations with visibilities between 0.09–0.35. If we assume a Gaussian intensity distribution of the source the visibilities indicate an intensity FWHM of $\approx$ 20–25 mas (8.5 μm) and 32–38 mas (12.0 μm) which is in rough agreement with the extension of the small component of Simon et al. (1985). We note, that these visibilities, although not reaching the relatively high levels of most Herbig Ae/Be stars (e.g., Leinert et al. 2004, Preibisch et al., these proceedings) seem to be qualitatively different from the very low visibilities (0.01 –0.05) found for several of the other objects in our sample as well as recently reported for two other massive YSOs (de Wit et al. 2007, Vehoff et al., these proceedings). Still, to learn more about the potentially more complicated intensity structure, a simple Gaussian is not a sufficient ansatz (and physically not validated), especially if the object is strongly resolved by the interferometer. Further modelling is necessary for interpretation.

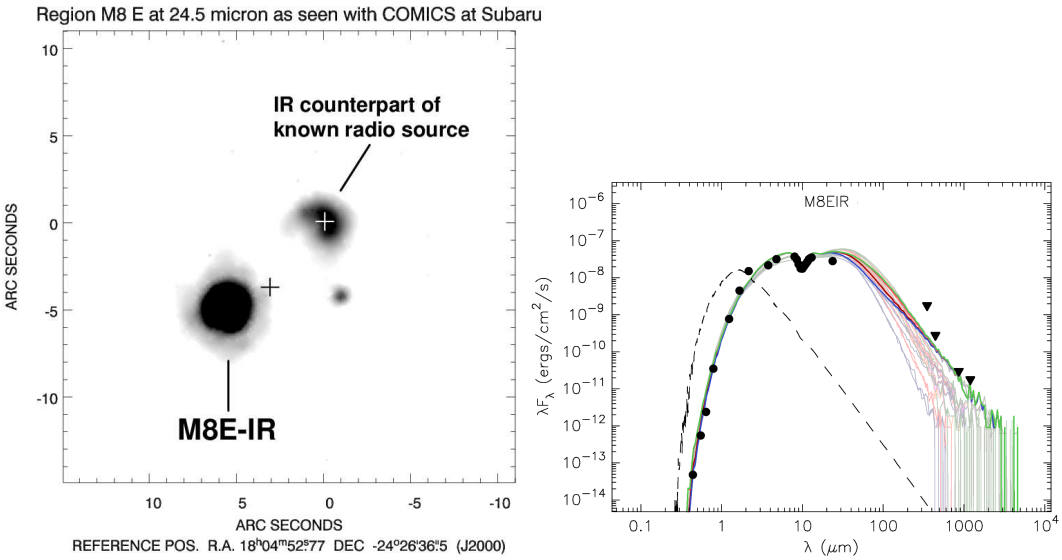

Figure 1. **Left:** Q-band image of the M8E region at 24.5 μm with COMICS/Subaru. The two previously known objects are annotated. The black plus indicates the position of a 44 GHz Methanol maser according to Val'tts (1999). The white plus marks the position of the cm continuum source (Molinari et al. 1998). **Right:** SED of M8E-IR. Black dots show observed fluxes while black triangles show upper limits. The continuous lines give the best-fitting radiative transfer model from the grid of models by Robitaille et al. (2007) (different curves for different synthetic aperture sizes). The dash-dotted curve shows the SED of the bloated central star of that model.

3.2. Modelling

We apply self-consistent continuum radiative transfer modelling to M8E-IR in order to produce synthetic MIR intensity maps and to compare their spatial frequency spectrum with the observed visibilities. Here, we are mainly concerned with the question which spatial distribution of the circumstellar material can account for both, the SED and the visibilities of M8E-IR.

For SED fitting, we use the M8E-IR photometric data collected in Mueller et al. (2002) plus new 1.2 mm data from Beltrán et al. (2006). We want to stress that no (sub-)millimeter interferometry on M8E-IR is reported in the literature which could spatially disentangle the flux contributions from M8E-IR and the radio source 8″ away. Hence, we consider the M8E-IR fluxes for $\lambda > 24.5\,\mu$m just as upper limits in our modelling. Furthermore, we include new optical photometry in the B, V, and I filters reported by Prisinzano et al. (2005, their object Cl* NGC 6530 WFI 13458) as well as our new 24.5 μm photometry. In addition, the 8–13 μm total flux spectrum taken in the course of the MIDI measurements (Sect. 2.) was used to further constrain the multitude of viable models.

We started with well-tested models where the parameters just show a radial dependence (Men'shchikov et al. 1999). With a purely spherically symmetric geometry and a hot central star it was already possible to find models that reasonably fit the optical to MIR SED of M8E-IR. Furthermore, the modelling is

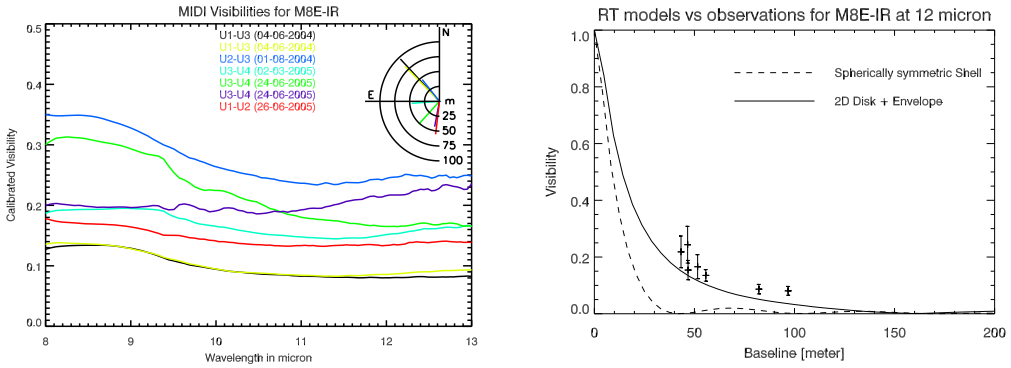

Figure 2. **Left:** Collection of dispersed MIDI visibilities. The inset schematically shows the baseline lengths and orientations (cf. Table 1). **Right:** Comparison of the spherically symmetric model incl. a hot central star and the full 2D model with envelope + disk + bloated cool star. Given are cuts through the 12 μm model images with the resulting visibilities over the spatial frequencies (in units of the interferometric baseline length). MIDI data for the 7 baselines are also plotted as plus signes including the formal 3σ error bars for comparison.

capable of disentangling the principle contributions from M8E-IR and the neighbouring radio source to the total energy budget by assuming and modelling two distinct components. M8E-IR dominates up to wavelengths of $30-40$ μm. To the total luminosity of around $1.7-2.0 \times 10^4$ $L_\odot$ (cf. also Mueller et al. 2002), M8E-IR might contribute less than 50%. Still, compared to the measured visibilities, these models resulted in far too low visibilities (< 0.05) for M8E-IR in the baseline range 30–60 m over the whole 8–13 μm range. The error margins of the MIDI visibilities ($\approx$ 10%) do not account for such large differences (Fig. 2). Hence, we extended our parameter search to full 2D models. We used the SED online fitting tool of Robitaille et al. (2007) to include models with envelope + circumstellar disk. We refer to this publication for details on the setup of these models. The best fits point to models comprising a very compact circumstellar disk (< 50 AU) and a larger surrounding envelope with small bipolar cavities. Due to the linkage of the Robitaille grid to evolutionary tracks, certain size parameters cannot be independently chosen by the fitter (see Robitaille, these proceedings). This especially affects the possible disk size which is not well constrained in our case. The data would still allow for a somewhat larger disk. Note however, that for disk radii clearly larger than 100 AU, the MIR visibilities eventually drop. We mention explicitly, that among the fitting models there are also configurations without a disk (axisymmetric flattened envelope + outflow cavities only), which nevertheless give similarly high visibilities. This suggests that in the case of M8E–IR, the choice of the central object might actually govern the resulting visibility levels (see below). In Fig. 1 (Right) we show the best SED fit to M8E-IR by the Robitaille models. In Fig. 2 (Left) the u,v-spectrum of the 12 μm synthetic image based on this model is included as a solid line. It is compared to the corresponding image from the above-mentioned spherically symmetric modelling (dashed line). Although the u,v-spectrum of the 2D model

still shows somewhat lower visibilities than the measured ones, obviously it is qualitatively different from the spherically symmetric model. Due to the low inclination of the best 2D model (18°), the central intensity distribution shows only small deviations from radial symmetry. Hence, differences in the model visibilities with varying position angle remain small ($< 10\%$), and the cut shown in Fig. 2 can be adopted as representative. We explicitly mention the low inclination angle of $< 30°$ inherent in all our 2D models that fit the SED data. This is in contrast to the disk hypothesis of Simon et al. (1985) that featured a very large inclination. However, Simon et al. saw a more or less symmetric intensity distribution in their 10 μm lunar occultation data; hints for deviations came mainly from lunar occultations recorded at 3.8 μm. At this shorter wavelength, configurations with disk + envelope incl. outflow cones are naturally more structured, and scattered light in the inner regions of these cones can still contribute, in particular if grains larger than the typical 0.1 μm dust particles are involved. Interestingly, the best-fitting models for M8E-IR in the Robitaille model grid features central stars of 10–15 $M_\odot$ which are strongly bloated (120 – 150 $R_\odot$) and, therefore, have relatively low effective temperatures. Such solutions can occur since the Robitaille grid also comprises the full range of canonical pre-main sequence evolutionary tracks from the Geneva group[2] as possible parametrisation of the central objects. M8E-IR probably cannot straightforwardly be identified with correspondingly very early evolutionary stages, and we again refer to the contribution by Robitaille (these proceedings) for an extensive discussion on the intricate dependencies in his model grid. However, the tendency for a bloated central star in the case of M8E-IR may be valid. As mentioned already in Kippenhahn & Meyer-Hofmeister (1977), accretion with high rates onto main sequence stars can temporarily puff up such stars (see also Zinnecker & Yorke 2007). Further encouragement to consider this comes from contributions presented during this conference (Hosokawa and Omukai as well as Yorke and Bodenheimer, these proceedings). These authors compute the pre-main-sequence evolution of stars in dependence of the accretion rate and find that for accretion rates (onto the forming star) reaching $10^{-3}\,M_\odot$/yr, the protostellar radius can temporarily increase to $> 100\,R_\odot$, in accordance with our indirect findings from the model fitting. Interestingly, Mitchell et al. (1988) revealed high-velocity molecular outflows from M8E-IR based on M-band CO absorption spectra and speculated on recent (< 120 yr) FU Ori-type outbursts for this object. If these multiple outflow components really trace recent strong accretion events, the central star could have indeed been affected. Furthermore, M8E-IR is not detected by cm observations with medium sensitivity (Simon et al. 1984; Molinari et al. 1998). This could be explained by large accretion rates still quenching a forming hypercompact HII region (e.g., Walmsley 1995). However, also a bloated central star with $T_{\rm eff} \ll 10000$ K would give a natural explanation for these findings.

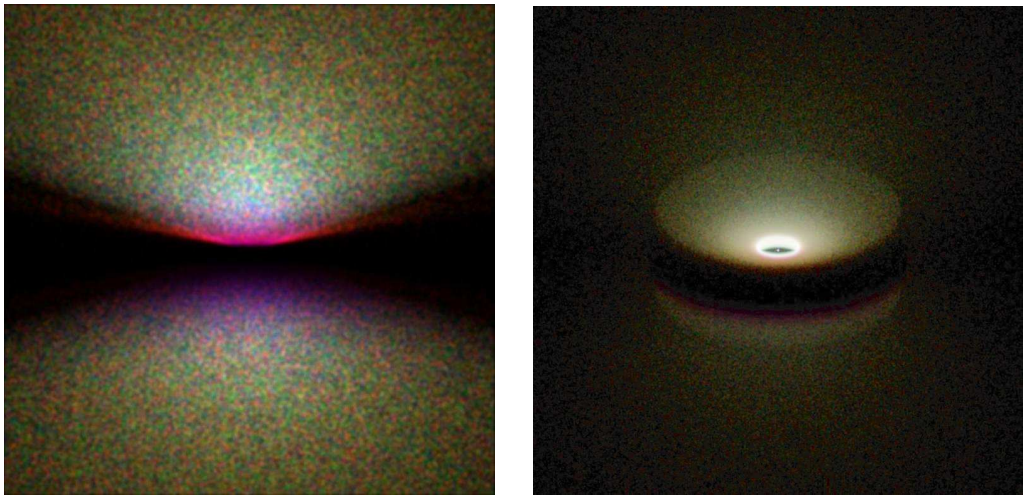

Figure 3. Synthetic 8 – 13 μm images (in logarithmic stretch) for the two best-fitting models delivered by the Robitaille fitter for M 17 IRS1. Both images display a linear size of 2000 × 2000 AU^2. **Left:** Nearly edge-on model with inclination angle 87°, a disk radius of 2720 AU and a 17.5 $M_\odot$ central star with $T_{\rm eff}$ = 33400 K. **Right:** Model with inclination angle 63°, a disk radius of 525 AU and a 7.9 $M_\odot$ central star with $T_{\rm eff}$ = 15800 K. This model fits the measured visibilities much better than the other model.

4. A new look onto M 17 IRS1

In order to give another example for the abilities of MIR interferometry to assess the viability of different geometric models for a massive YSO, we briefly mention our preliminary results for the object M 17 IRS1 (e.g., Chini et al. 2004). Here, we have obtained three visibility measurements with different position angles for baselines from 43 m to 56 m. We find clearly different visibility levels for the three measurements, staying at a 0.05-level for one measurement but reaching about 0.3 for the two other ones. Also here, we consulted the Robitaille SED fitter in order to find models reproducing the SED. Since the SED of M 17 IRS1 is less constrained in the literature than in the case of M8E-IR, the fitter allows for a larger variety of models, all however including an intermediate-sized circumstellar disk. In Fig. 3 we show two of the best-fitting models. It gets obvious that in the 87° edge-on model to the left we see relatively diffuse emission only, since the central source is hidden by the outer disk. Consequently, this model results in far too low N-band visibilities and does *not* reach the measured visibility levels of 0.2 – 0.3 for any baseline orientation. The less inclined 63° model to the right at least provides a direct view onto the inner hot disk rim and therefore results in clearly higher visibilities than the edge-on model.

[2] `http://obswww.unige.ch/~mowlavi/evol/stev_database.html`

5. Conclusion

We have observed massive young stellar objects with the MIR interferometer MIDI at the VLTI. We find substructures with MIR sizes around 30 – 50 mas. Using the measured visibilities as discriminator, we can exclude purely spherically symmetric matter distributions with a hot central star for the object M8E-IR. The most probably configuration consists of a compact circumstellar disk surrounded by a larger envelope, although the total disk size is not well constrained by the models. Until (sub-)millimeter observations with sufficient spatial resolution better constrain the emission at long wavelength, disks with radii from 20–100 AU seem probable. Furthermore, our data are consistent with the view that M8E-IR harbours a 10–15 $M_\odot$ central star that has been bloated by recent strong accretion events. Both aspects should be the topic of future investigations, for instance by utilising IR spectroscopy.
For M 17 IRS1, we can exclude the nearly edge-on disk model which had been suggested by the best-fitting 2D SED model. Instead, a moderately inclined circumstellar disk might be closer to the truth, and the results support an earlier suggestion that M 17 IRS1 is a kind of still embedded Herbig Be star.
Our results show that IR interferometry is a viable tool to reveal decisive structure information on embedded MYSOs and to resolve ambiguities arising from fitting the spectral energy distribution. With the inclusion of the auxiliary telescopes, the VLTI is currently becoming even more flexible to tackle such tasks. Finally, 2nd-generation VLTI instruments like MATISSE (Lopez et al. 2006) for the thermal IR will reveal even more complex details of MYSOs by adding imaging capabilities to MIR interferometry.

Acknowledgments. Discussions with Th. Robitaille, B. Whitney, and M. Hoare are appreciated.

References

Arias, J. I., Barbá, R. H., & Morrell, N. I. 2007, MNRAS, 374, 1253
Baba, H., Yasuda, N., Ichikawa, S.-I., et al. 2002, in ASP Conf. Ser. 281, D. A. Bohlender et al. (eds.), 298
Beltrán, M. T., Brand, J., Cesaroni, R., et al. 2006, A&A, 447, 221
Chini, R., Hoffmeister, V. H., Kämpgen, K., et al. 2004, A&A, 427, 849
De Buizer, J. M. 2006, ApJ, 642, L57
de Wit, W. J., Hoare, M. G., Oudmaijer, R. D., Mottram, J. C. 2007, ApJ, 671, 169
Henning, T. 1990, Fundamentals of Cosmic Physics, 14, 321
Kippenhahn, R. & Meyer-Hofmeister, E. 1977, A&A, 54, 539
Leinert, C., Graser, U., Waters, L. B. F. M., et al. 2003, Proc. SPIE, 4838, W. A. Traub (ed.), 893
Leinert, C., van Boekel, R., Waters, L. B. F. M., et al. 2004, A&A, 423, 537
Linz, H., Stecklum, B., Henning, T., Hofner, P., & Brandl, B. 2005, A&A, 429, 903
Lopez, B., et al. 2006, Proc. SPIE, 6268, J. D. Monnier et al. (eds.), 31
Men'shchikov, A. B., Henning, T., & Fischer, O. 1999, ApJ, 519, 257
Mitchell, G. F., Allen, M., Beer, R., et al. 1988, ApJ, 327, L17
Mitchell, G. F., Hasegawa, T. I., & Schella, J. 1992, ApJ, 386, 604
Molinari, S., Brand, J., Cesaroni, R., Palla, F., & Palumbo, G. 1998, A&A, 336, 339
Mueller, K. E., Shirley, Y. L., Evans, II, N. J., & Jacobson, H. R. 2002, ApJS, 143, 469

Okamoto, Y. K., Kataza, H., Yamashita, T., et al. 2003, in Instrument Design and Performance for Optical/Infrared Ground-based Telescopes. Proc. SPIE, Vol. 4841, ed. M. Iye & A. F. M. Moorwood, 169–180
Prisinzano, L., Damiani, F., Micela, G., & Sciortino, S. 2005, A&A, 430, 941
Robitaille, T. P., Whitney, B. A., Indebetouw, R., & Wood, K. 2007, ApJS, 169, 328
Simon, M., Cassar, L., Felli, M., et al. 1984, ApJ, 278, 170
Simon, M., Peterson, D. M., Longmore, A. J., Storey, J. W. V., & Tokunaga, A. T. 1985, ApJ, 298, 328
Val'tts, I. E. 1999, Astronomy Reports, 43, 149
Walmsley, M. 1995, in Rev. Mex. Astron. Astrofis. (Conf. Series), Vol. 1, 137
Zinnecker, H. & Yorke, H. W. 2007, ARA&A, 45, 481